

## Macromagnetism and micromagnetism in Ni-Mo metallic superlattices

J. W. Cable

*Oak Ridge National Laboratory, Oak Ridge, Tennessee 37830*

M. R. Khan,\* G. P. Felcher, and Ivan K. Schuller

*Argonne National Laboratory, Argonne, Illinois 60439*

(Received 6 March 1986)

The magnetic properties of Ni-Mo metallic superlattices have been examined by magnetization and polarized-neutron diffraction measurements. The samples are ferromagnetic, with an ordering temperature rapidly increasing with the superlattice period  $\Lambda$ . The saturation magnetization per nickel atom also increases with  $\Lambda$ , gradually approaching the value of the pure metal. The proximity of molybdenum lowers the nickel magnetic moments with a deeper perturbation at the imperfections of the crystalline layers. A comparison of x-ray and neutron scattering data implies that the magnetic profile in the superlattice is more perfect than the chemical profile.

### I. INTRODUCTION

Considerable interest has been developing in recent years<sup>1,2</sup> on the magnetic properties of thin films and their relation with the magnetism of the same metals in bulk form. Films a few tens of angstroms thick are comparable to the range of the magnetic interactions, hence any magnetic order in the bulk is deeply modified by the surfaces. If the thin film of normally magnetic metal is sandwiched between thick layers of a normally nonmagnetic metal, the magnetic properties of the film may change drastically, as a result of the structural and electronic mismatch of the two metals. A further variation of the composite sandwich is a metallic superlattice, in which layers of a magnetic metal are alternated periodically with layers of a nonmagnetic metal. The magnetic state of the material depends on the magnetic interactions both within and between the layers, and these interactions are in turn dependent on the layer thickness and the inter-layer distance. In principle, these two quantities can be changed at will by controlling the conditions of the sample preparation.

Neutron diffraction can determine not only the chemical and structural, but also the magnetic modulation of a metallic superlattice.<sup>3,4</sup> This is possible if the real material under study is close to an ideal superlattice; for less-perfect samples, diffraction measurements provide a less-detailed microscopic picture, against which to compare the macroscopic magnetic properties.

The nickel-molybdenum system offers a good test of the magnetic behavior of superlattices. A fair amount of information is already at hand on the magnetic response of nickel in proximity to nonmagnetic atoms. Alloying nickel with molybdenum causes a sharp drop of the Curie temperature and of the magnetization;<sup>5</sup> the decrease of both quantities (roughly linear with Mo concentration) is such that for 9 at. % Mo the alloy is nonmagnetic. Diffuse neutron scattering measurements showed that isolated molybdenum atoms strongly depress the magnetic moments of the adjacent Ni up to the second neighbor cell.<sup>6,7</sup>

A similar perturbation is caused by most metallic impurities in nickel. At interfaces with nonmagnetic metals it seems (from measurements of the anomalous Hall coefficient) that nickel is also magnetically dead for a depth of two atomic planes.<sup>8</sup> All present evidence indicates that molybdenum, at least in its metallic form, does not have a local magnetic moment.

The layered materials 1  $\mu\text{m}$  thick were grown by sputtering on a variety of substrates including mica, 90° sapphire, and (111) silicon wafers. X-ray analysis shows that the superlattice modulation period  $\Lambda$  is close to that monitored during the growth; in this period layers of Ni of thickness  $D_{\text{Ni}}$  are alternated with layers of Mo of thickness  $D_{\text{Mo}}$  with very little interdiffusion. The crystalline state of the films (whose details will be discussed later) is similar for samples grown on different substrates; hence, it is reasonable to assume that their magnetic properties are also substrate independent, and are characterized solely by the thicknesses of the Ni and Mo layers.

### II. MAGNETIZATION MEASUREMENTS

Measurements were done on a series of samples of varying nickel and molybdenum layer thicknesses. Most of the samples were grown with equal thickness layers ( $D_{\text{Ni}} = D_{\text{Mo}}$ ); however, samples were also prepared with  $D_{\text{Ni}} = 3D_{\text{Mo}}$  and  $3D_{\text{Ni}} = D_{\text{Mo}}$ . The films grown on mica were lifted off by slow immersion in a mixture of water and alcohol at a tilt angle. The surface tension of the liquid is sufficient to lift off the clean metal (as shown by x-ray scattering); in contrast, mechanical stripping leaves a considerable amount of mica adhered to the metal. The lifted samples, of  $\sim 0.1$  mg weight, were placed in a calibrated aluminum container and inserted in the magnetometer with the magnetic field parallel and perpendicular to the film. The measurements were calibrated against a platinum standard, and corrected for the signal of the empty aluminium container. The SQUID magnetometer (SHE VTS 10) was capable of a maximum field of 10 kOe and a temperature range of 5–400 K.

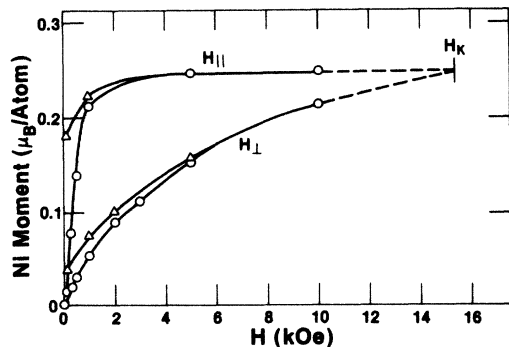


FIG. 1. Magnetization of an equal thickness Ni-Mo superlattice,  $\Lambda=50$  Å at 5 K, for a magnetic field applied parallel and perpendicular to the film. Open circles: increasing field. Triangles: decreasing fields.

A typical magnetization curve is presented in Fig. 1. The  $\Lambda=50$  Å equal thickness superlattice shows, in a parallel field and at 5 K, the characteristic magnetic behavior of a good ferromagnet with a well-defined saturation value (well below that of pure nickel) and a remanent magnetization  $\sim 75\%$  of the saturation value. The phenomenology of the magnetization process is quite similar to that found for Cu-Ni superlattices.<sup>9-11</sup> Thus, when the magnetic field is applied perpendicular ( $H_{\perp}$ ) to the film the magnetization approaches saturation almost linearly. The extrapolated intercept of the magnetization curves for  $H_{\parallel}$  and  $H_{\perp}$  occurs at a field  $H_K=4\pi M_0 + 2K_u/M$ , where the first term represents the demagnetizing field, and  $K_u$  is the anisotropy constant which, if positive, indicates that the easy axis is in the plane of the film. This is indeed the case for the Mo-Ni superlattices; for example, for  $\Lambda=50$  Å (cf. Fig. 1)  $2K_u/M=12.6$  kOe. Similarly to the Cu-Ni superlattices, the anisotropy increases with decreasing  $\Lambda$ .

The spontaneous magnetization (extrapolated to  $T=0$ ) for a series of samples is presented in Fig. 2 as a function of the Ni layer thickness. The superlattices are not ordered magnetically below  $D_{Ni}\sim 8$  Å, [approximately equal to four Ni(111) interatomic]; for increasing layer thickness, the magnetic moment approaches, without reaching the value for bulk Ni metal. In addition there is a consistent decrease of the magnetic moment per nickel in samples containing thicker molybdenum layers.

The Curie temperatures were obtained from isothermal magnetization curves in the form of Arrott plots ( $M^2$  versus  $H/M$ ). For homogeneous systems, the Arrott plots are straight lines, parallel to each other, for different temperatures, with that at  $T=T_c$  intercepting the origin. A comprehensive treatment has not been given yet for heterogeneous systems. Random concentration fluctuations in a weak itinerant ferromagnet add terms in the expression of the free energy that cause a curvature in the Arrott plots.<sup>12</sup> At the other extreme, periodic magnetic superlattices have been treated neglecting interlayer interactions.<sup>13</sup> Our experimental results—of which a typical example is shown in Fig. 3—are approximately straight lines; and we define empirically as a “Curie temperature”

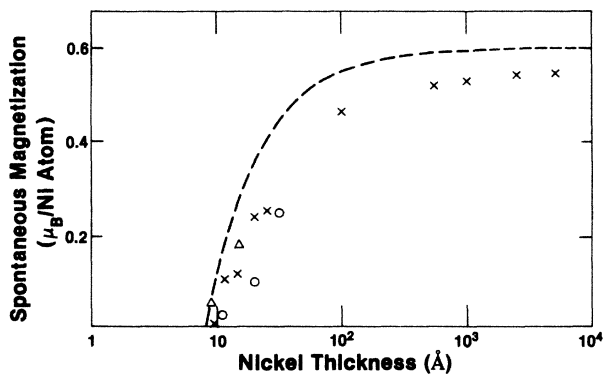


FIG. 2. Spontaneous magnetization at  $T=0$  of Ni-Mo superlattices, as a function of the nickel layer thickness. Crosses:  $D_{Ni}=D_{Mo}$ . Triangles:  $D_{Ni}=3D_{Mo}$ . Open circles:  $D_{Mo}=3D_{Ni}$ . Dashed curve: magnetization for a model in which the nickel layer has two outer atomic planes magnetically dead and the center magnetic moments are equal to those of pure nickel.

that whose isotherm intercepts the origin. The Curie temperatures are presented in Fig. 4 as a function of the nickel magnetization. The points seem to fall on a common curve, regardless of the Mo layer thickness. For low magnetization values,  $T_c$  is linear with  $\mu_{Ni}$ , extrapolating to the values for pure nickel. However, for higher values of  $\mu_{Ni}$ ,  $T_c$  increases dramatically beyond the maximum temperature allowed by our experimental setup.

The magnetization results cannot be easily fitted to a simple model. The rapid rise of the Curie temperature with the nickel moment is not unexpected in strongly heterogeneous systems such as superlattices. It indicates that even in fairly thin layers, the magnetic interactions have a strength comparable to that of pure nickel. Nevertheless, the average magnetic moment is still well below that of pure nickel. Even invoking the presence of a magnetically dead layer, at the Ni-Mo interface—as in the curve drawn in Fig. 2—an unsatisfactory agreement is found with the experiment. In order to shed light on the

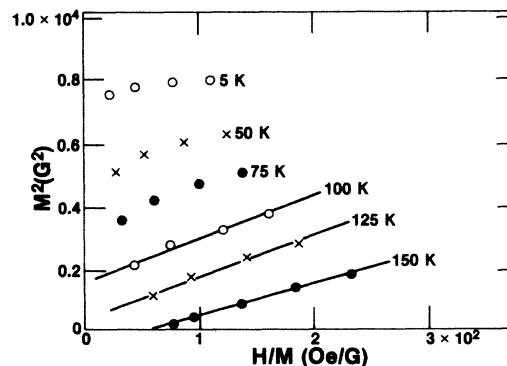


FIG. 3. Arrott plots for an equal thickness Ni-Mo superlattice of  $\Lambda=23.4$  Å. The magnetization values are defined in terms of the Ni present and not the total volume.

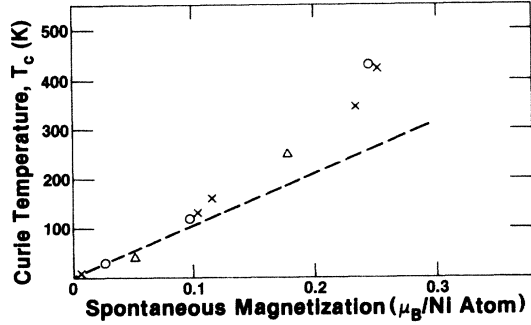


FIG. 4. Curie temperature versus nickel moment for Ni-Mo superlattices of different relative thicknesses (symbols as in Fig. 2). The dashed straight line extrapolates to the  $T_c$  and  $\mu$  values for pure nickel.

actual magnetic (and structural) modulation in these materials, a series of diffraction experiments was undertaken.

### III. DIFFRACTION THEORY

The theory of diffraction (of x rays or neutrons) by artificial superlattices has been discussed extensively by de Fontaine<sup>14</sup> and McWhan.<sup>15</sup> Assume an ideal situation in which there is perfect modulation of nickel and molybdenum of period  $\Lambda = D_{\text{Ni}} + D_{\text{Mo}}$  in the direction normal to the film ( $z$  direction). In the reflection geometry (scattering vector normal to the surface; sample and detector rotated with a coupled  $\theta$ - $2\theta$  motion) diffraction lines appear at  $2 \sin \theta / \lambda = n / \Lambda$ , where  $\lambda$  is the neutron (or x-ray) wavelength and  $n$  is an integer. The structure factor that gives rise to the intensity of the  $n$ th diffraction peak is

$$F \left[ \frac{n}{\Lambda} \right] = \frac{1}{\Lambda} \int_0^\Lambda b(z) \rho(z) \exp \left[ 2\pi i \frac{nz}{\Lambda} \right] dz, \quad (1)$$

where  $b(z)$  and  $\rho(z)$  are, respectively, the atomic scattering amplitude and the atomic density at the position  $z$ . The  $F(n/\Lambda)$  are the Fourier coefficients of the function  $b \cdot \rho$ , which can be determined with a  $z$  resolution increasing with the number of measured lines.

It is important to examine how structural imperfections perturb the amplitudes of the diffraction peaks and degrade the information that can be obtained from them. A narrow Bragg reflection implies a coherence range (in the  $z$  direction) of several modulation wavelengths. Within this range, an average is made of the scattering amplitude for all the planes with the same phase  $s + n\Lambda$ . Different types of lattice inhomogeneities are involved in the averaging process: missteps of the nickel-molybdenum interfaces, local tilts of the layers, or an imperfect  $\Lambda$  periodicity. All these structural imperfections decrease the *diffracted intensities* in the same way as if interdiffusion had occurred, forming alloys of appropriate compositions at each equiphase plane. Yet, the detailed physical pictures are quite different, and they are expected to give rise to different magnetic behavior. Only a complete diffraction analysis, including the intensity of the off-axis reflections,

and a careful evaluation of the relative linewidths would enable one to discriminate between different kinds of disorder.

In Eq. (1) the density of the particles  $\rho(z)$  is not necessarily a smooth function of  $z$  with period  $\Lambda$ ; although this approximation is valid for small values of the scattering vector, it certainly breaks down for  $2 \sin \theta / \lambda \sim 1/d$ , when  $d$  is an interatomic lattice spacing of the materials. In a textured material, Ni and Mo grow with a definite crystal orientation in the  $z$  direction. The lattice sum

$$F(k) = \frac{1}{L} \sum_{m=1}^{L/\bar{d}} b_m \exp(ikz_m) \quad (2)$$

has a maximum at  $k = 2\pi/\bar{d}$ , where  $\bar{d}$  is the average lattice spacing,  $b_m$  is the scattering amplitude per unit area of the plane located at  $z_m$ , and  $L$  is the coherence length.

The deviation  $\epsilon_m$  of the  $m$  atomic plane from its average position is given by  $z_m = \epsilon_m + m\bar{d}$ . Expanding both  $b_m$  and  $\epsilon_m$  in a Fourier series, with the fundamental period equal to  $\Lambda$ :

$$b_m = \bar{b} + \sum_{-\infty}^{\infty} \Delta b_n \exp \left[ 2\pi i n \frac{z_m}{\Lambda} \right], \quad (3a)$$

$$\epsilon_m = \sum_{-\infty}^{\infty} \eta_n \exp \left[ 2\pi i n \frac{z_m}{\Lambda} \right], \quad (3b)$$

and substituting in the lattice sum, Eq. (2), one finds additional maxima at the positions  $2 \sin \theta / \lambda = 1/d \pm l/\Lambda$ , where  $l$  is an integer. These new Bragg reflections may be called satellites of the reflection  $1/d$ , and those described in Eq. (1) satellites of the origin. In a perfect superlattice the positions of the two sets of satellites should be consistent, otherwise  $\Lambda$  consists of a noninteger number of atomic planes.

The structure factors of the satellites can be presented in an explicit, but approximate analytical form in some special cases. For instance, for an equal thickness superlattice ( $D_{\text{Ni}} = D_{\text{Mo}}$ ), retaining only the first harmonic of the expansions in Eqs. (3), the structure factor of the  $(1/\bar{d})$  group of reflections is

$$k = \frac{2\pi}{\bar{d}}, \quad F = \bar{b} [J_0(k\eta_1)], \quad (4a)$$

$$k = 2\pi \left[ \frac{1}{\bar{d}} \pm \frac{1}{\Lambda} \right], \quad (4b)$$

$$F = \bar{b} [J_1(k\eta_1)] \pm \Delta b_1 \left[ \frac{1}{2} J_0(k\eta_1) + \frac{1}{4} J_2(k\eta_1) \right],$$

$$k = 2\pi \left[ \frac{1}{\bar{d}} \pm \frac{2}{\Lambda} \right], \quad (4c)$$

$$F = -\bar{b} [J_2(k\eta_1)] \mp \Delta b_1 \left[ \frac{1}{2} J_1(k\eta_1) \right].$$

Equations (4) have an interesting structure. The terms in square brackets represent the lattice modulation, while their coefficients are the average and the periodic fluctuations of the scattering amplitudes. Such a formulation retains its validity beyond the approximations used to derive the detailed expressions. For instance, the lattice modulations can be calculated exactly (rather than approximated

by Bessel functions) from sums of the periodical lattice. Random disorder has the following effects: a disorder in amplitude decreases the values of  $\Delta b$ ; instead, a disorder of the phases gives rise to a correcting term which has the form of a Debye-Waller factor.

The above considerations are valid both for x-ray and neutron scattering, as long as the proper scattering amplitudes are used. For neutrons, both the nuclear ( $b$ ) and magnetic ( $p$ ) amplitudes have to be considered. In a typical polarized neutron experiment, the sample is saturated by a magnetic field  $H$  parallel to the film and normal to the scattering vector. For neutrons polarized parallel (+) or antiparallel (-) to  $H$ , the scattering amplitudes are, respectively,  $b \pm p$ . Since  $p(z)$  is proportional to the local magnetization  $\mu(z)$ , polarized neutron diffraction can in principle determine the complete magnetic and crystal modulation. However, this is a formidable task since  $p$ , is expected to vary, even in a perfect superlattice, as a function of the position of the atoms in the magnetic layer and in particular their distance from the interface. Hence, the structural modulation is usually analyzed by x rays, and those findings are compared for consistency with those obtained by the polarized neutron method.

#### IV. DIFFRACTION EXPERIMENTS

##### A. Summary of the x-ray results

Extensive x-ray measurements were taken of the Ni-Mo superlattices.<sup>16</sup> In particular, the intensities of the  $1/\bar{d}$  group of reflections were analyzed and found to be in excellent agreement with a simple model, in which layers

of (110) planes of bcc Mo alternate with layers of (111) planes of fcc Ni. The interplane spacings are close to those of the respective metals; their symmetry, or lateral arrangement, was confirmed by off-axis diffraction patterns. The incommensurability of the modulation period  $\Lambda$  with the lattice spacings  $d_{\text{Ni}}$ ,  $d_{\text{Mo}}$  was simulated by introducing a thickness variation in the direction of growth; to achieve consistency with the experimental results, these faults had to be limited to one atomic plane at the interface. However, the samples could not yet be considered an ideal superlattice. In the plane of the film, they are composed of crystallites in registry over only a few tens of angstroms. In the direction normal to the film, the width of the rocking curves of the  $1/\bar{d}$  Bragg reflections indicates a spread of  $\sim 5^\circ$  around the main texture direction. Thus, the analysis of the x-ray intensities at large scattering angles ensures only that the crystallites forming the sample are individually well defined in the direction of growth; however, these crystallites are misoriented relative to each other, as illustrated in exaggerated form in Fig. 5. At small scattering angles, a few checks were done with x-rays: for films of nominal equal thickness in Ni and Mo, the second-order satellite was absent [as expected from Eqs. (1) and (3a)] while the third-order satellite was readily visible. The latter observation indicates that the chemical modulation is not entirely sinusoidal. However, no quantitative analysis was done of the chemical profile, since this requires an accurate comparison of the intensities of the third- versus the first-order satellite, which is severely affected by extinction. In contrast to the x-rays, the weaker scattering amplitude of neutrons allows relatively extinction-free measurements of the intensity of this satellite [even for the most intense (000)<sup>+</sup> reflections, the extinction was estimated to be less than 10%].

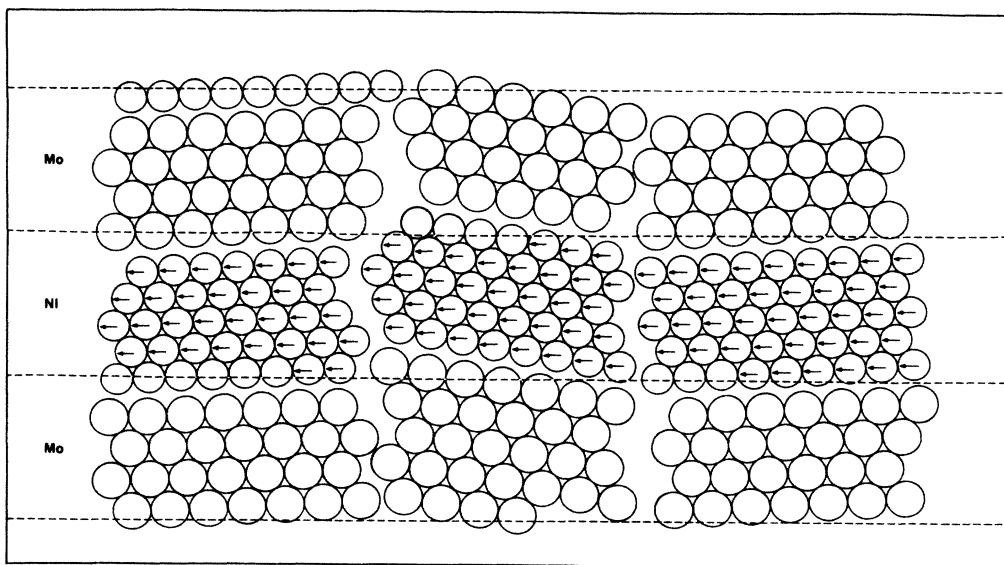


FIG. 5. Crystalline form of the Ni-Mo samples (small circles, Ni; larger circles, Mo). Three grains are shown with different exaggerated tilts to the film axis. These grains diffract x rays or neutrons independently at large angle. The dashed lines separate the Ni from the Mo sites; the small circles containing an arrow are the Ni with a magnetic moment.

### B. Polarized neutron experiments

The measurements were performed at the polarized neutron unit of the High Flux Isotope Reactor in Oak Ridge. The samples used were equal thickness films  $\sim 1 \mu\text{m}$  thick deposited on  $90^\circ$  sapphire substrate of 0.5 in. diameter. Sapphire was chosen because among the available substrates it was the one that gave no diffraction lines in the region of interest. The samples were mounted on a vanadium plate, and inserted in all-aluminum cryostat equipped with a superconducting magnet; the system was operated at  $T=4.2 \text{ K}$ , and  $H=5 \text{ kOe}$  applied in the plane of the films. Neutrons of  $1.5 \text{ \AA}$  wavelength were used. Table I shows a compendium of the measurements, given as the ratio  $I^+/I^-$ , or "flipping ratio."

In view of the imperfect texture of the sample (indicated by the width of the rocking curve) the diffraction lines of the  $1/\bar{d}$  group were found to be weak and superimposed on a sizable background due to neutrons scattered by the structural components. Most prominent was the diffraction pattern of aluminum of the cryostat, although care was taken to avoid aluminum in the immediate vicinity of the sample. The background was defined as the scattered intensity at the wings of the rocking curves. The weakness of the reflections and the large correction for the background are responsible for the statistical error in the flipping ratios of the group of lines around  $1/\bar{d}$ . In contrast, the first satellite of the origin was easy to detect and its flipping ratio was determined much more accurately.

### C. Analysis of the (000)<sup>+</sup> satellite

It is easy to compare the flipping ratio of the (000)<sup>+</sup> satellite with that expected for a square-wave modulation of Ni and Mo. From Eq. (1) it can be derived

$$I^+/I^- = \left( \frac{1+\gamma}{1-\gamma} \right)^2 \quad (5)$$

with

$$\gamma = \frac{\rho_{\text{Ni}}}{\frac{\Lambda}{\pi}(b_{\text{Ni}}\rho_{\text{Ni}} - b_{\text{Mo}}\rho_{\text{Mo}})} \int_0^{\Lambda/2} p(z)\cos\left(\frac{2\pi z}{\Lambda}\right) dz. \quad (6)$$

TABLE I. Flipping ratios for equal thickness Ni-Mo superlattices. The numbers in parenthesis indicate the experimental errors in the last significant digit.

Reflections ( $k/2\pi$ )	$\Lambda=28.5$	$40.4 \text{ \AA}$	$50.9 \text{ \AA}$	$83.6 \text{ \AA}$
$1/\Lambda$	1.63(3)	2.26(2)	2.56(3)	2.46(4)
$\frac{1}{\bar{d}} - \frac{2}{\Lambda}$				0.91(6)
$\frac{1}{\bar{d}} - \frac{1}{\Lambda}$	1.04(10)	0.94(2)	0.89(3)	1.05(4)
$\frac{1}{\bar{d}}$	1.09(3)	1.16(2)	1.22(3)	1.05(6)
$\frac{1}{\bar{d}} + \frac{1}{\Lambda}$	1.099(6)	1.15(4)	1.26(3)	1.24(4)
$\frac{1}{\bar{d}} + \frac{2}{\Lambda}$		1.07(3)	1.19(6)	1.23(9)

For small scattering angles, the magnetic part is simply  $p(z)=c\mu(z)$ , where

$$c = \frac{eh}{mc^2} (0.2695 \times 10^{-12} \text{ cm}/\mu_B)$$

and  $\mu(z)$  is the atomic magnetization. (Mo is not expected to have an appreciable magnetic moment.) With the tabulated values of the nuclear scattering amplitudes and the metallic densities ( $b_{\text{Ni}}=1.025 \times 10^{-12} \text{ cm}$ ,  $b_{\text{Mo}}=0.688 \times 10^{-12} \text{ cm}$ ;  $\rho_{\text{Ni}}=0.0925 \text{ \AA}^{-3}$ ,  $\rho_{\text{Mo}}=0.0646 \text{ \AA}^{-3}$ ) the flipping ratio can be calculated for any distribution of magnetic moments for which the average  $\bar{\mu}_{\text{Ni}}$  is determined by the magnetization measurements. Figure 6 illustrates the results of such calculations: the lower boundary curve is obtained by assuming all the Ni moments equal; the upper boundary is for a moment concentrated at the physical center of the Ni layer. The latter curve is the highest flipping ratio that can be obtained for any distribution of the Ni moments, consistent with the magnetization values. Since even for this (highly unphysical) distribution, the calculated flipping ratios are lower than measured, it has to be concluded that the starting hypothesis of a square-wave modulation is incorrect.

As discussed previously, the x-ray intensities for reflections of the  $1/\bar{d}$  group are explained in terms of an ensemble of fairly perfect crystallites which, however, are misoriented compared to each other, as illustrated in Fig. 5. For the satellites of the origin only the chemical modulation matters and this is strictly normal to the plane of the film; a tilt from this axis should quickly destroy the interference pattern as indeed is evidenced by the sharp-

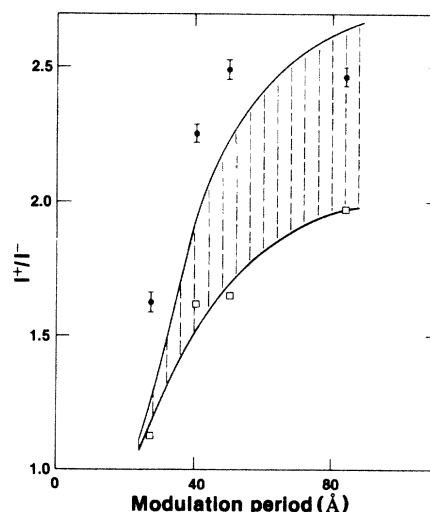


FIG. 6. Experimental flipping ratio of the (000)<sup>+</sup> reflection of equal thickness Ni-Mo, compared with those calculated from magnetization measurements assuming a perfect superlattice. Open square: calculated flipping ratio for a uniform Ni magnetization. The points were joined by the lower boundary line. The upper boundary line is the flipping ratio calculated assuming all the magnetization at the center of the Ni layer. The band in between contains all possible models for which magnetization at the center of the Ni layers is higher than at the interface.

TABLE II. Magnetic moments (in Bohr magnetons) obtained from magnetization and neutron scattering experiments.

Modulation period (Å)	Magnetization per atom $\bar{\mu}$	Model I		Model II	
		$\bar{\mu}$	$\Delta\mu$	$\bar{\mu}$	$\Delta\mu$
28.5	0.06	0.060	0.060	0.080	0.005
40.4	0.12	0.085	0.085	0.100	0.070
50.9	0.13	0.150	0.150	0.130	0.140
83.6	0.17	0.150	0.150	0.149	0.147

ness of the rocking curve ( $0.2^\circ$ ) for this reflection.

The chemical modulation is not a square wave: each plane normal to the propagation axis slices through crystallites of different compositions. Thus, although it is still possible to identify Ni sites and Mo sites, it can be said that their interface is blurred at each side for a thickness  $\Delta z$ , which depends on this site of the crystallites and their tilt compared with the modulation axis. Now a distribution of Ni moments can always be found to fit both the magnetization and the neutron flipping ratios, provided that the moments assignment is not in a one-to-one relationship with the average local chemical structure.<sup>17</sup> Let us assume for instance that only these nickel atoms on the Ni sites are magnetically active, and for simplicity that they are all equal. The flipping ratios and  $\bar{\mu}_{\text{Ni}}$  can be fitted with a proper choice of  $\Delta z$ , the thickness of the interface. This turns out to be of the order of two atomic planes for all the measured samples. Of course, this magnetic distribution is not unique; however, *common to all possible models is the requirement that the average magnetic profile is more perfect than the chemical profile.*

#### D. Analysis of the large angle lines

As a consequence of the model proposed above, the *individual crystallites* forming the film are nearly perfect structurally, but magnetically imperfect: the magnetic moments at equivalent sites might be different. Let us see if there is evidence for this disorder.

From the experimental flipping ratios and the aid of Eq. (5) the ratio of the structure factors  $\gamma = F_m/F_n$  can be obtained.  $F_n$  is known on the basis of the x-ray results.  $F_m$  is a linear combination of the magnetic moments in the material, with coefficients that are also well known, if the magnetic amplitudes are as perfectly modulated as their nuclear counterpart. Initially the experimental  $\gamma$ 's were best fit assuming only one value for the Ni moments, obtaining an already reasonable agreement (Table II, model I). However, the variance between experimental and best-fitted values is, for the films with shorter modulation length, outside the statistical error; and the agreement does not improve by allowing a more general distribution of the magnetic moments of nickel in the layer. Two specific models were tried: in the first, the layer was divided into a center and an interface region with different moments and different relative thicknesses. In the

second model, the magnetic modulation in the structure was expanded into a Fourier series, of which the two lowest terms were retained.

The central assumption common to these methods of analysis, is that the magnetic moments are perfectly modulated within each crystalline grain. If some kind of disorder in the magnetic amplitudes is present, its effect on the diffracted intensities can be treated only approximately. The magnetic structure factor [Eq. (4)] contains terms proportional to the average magnetization,  $\bar{\mu}$ , and to the magnetic fluctuation with the modulation period,  $\Delta\mu$ , which only for a perfect modulation is equal to  $\bar{\mu}$ . A disorder in the magnetic amplitude does not affect  $\bar{\mu}$  but the moment fluctuations have to be analyzed in many components, of which only some are present in  $\Delta\mu$ ; hence,  $\bar{\mu}$  and  $\Delta\mu$  can be treated as independent quantities. The result of the least-squares analyses of the neutron intensities for  $\bar{\mu}$  and  $\Delta\mu$  is presented in the last column of Table II. Since the variance is in all cases smaller than the experimental error, it is not possible to define better the magnetic structure.

#### V. DISCUSSION

From the comparison of macroscopic and microscopic magnetic measurements, it is apparent that superlattices of Ni-Mo exhibit a ferromagnetic structure which is well modulated with the superlattice period. The magnetization within the layers grows with the superlattice period. However, the detailed behavior of the magnetic response of nickel in proximity of molybdenum has not been sorted out yet, and thus a detailed microscopic description of the behavior of the magnetization is not possible. This is due to the fact that the prepared samples are not yet perfect. In these circumstances, the polarized neutrons are used complementary to the x rays to define the crystalline configuration of the samples better. In regard to magnetism, neutrons have established that the magnetic modulation is more planar than the lateral corrugation of the lattice. This might be correlated with the magnetic anisotropy of the films. If so, even more drastic anisotropy should be observed in samples of higher perfection. The growth of such samples, although a very difficult task for metallic superlattices, does not seem out of reach, with the constant improvement of sophistication and reliability of the deposition techniques.

## ACKNOWLEDGMENTS

The present work was supported by the U.S. Department of Energy, in part under Contract No. DE-AC05-84OR21400 with Martin Marietta Energy Systems, in

part by the BES Materials Sciences, under Contract W-31-109-Eng-38, and by the U.S. Office of Naval Research under Grant No. 00014-83-F-0031. One of us (I.K.S.) would like to acknowledge useful conversations with J. Hirsch and L. Sham.

\*Present address: Stolle Corporation/Alcoa, Sidney, OH 45365.

<sup>1</sup>*Synthetic Modulated Structures*, edited by L. Cheng and B. C. Giessen (Academic, New York, 1985).

<sup>2</sup>*Dynamical Phenomena at Surfaces, Interfaces and Superlattices*, edited by F. Nizzoli, K. H. Rieder, and R. F. Willis (Springer-Verlag, Berlin, 1985).

<sup>3</sup>G. P. Felcher, J. W. Cable, J. Q. Zheng, J. B. Ketterson, and J. E. Hilliard, *J. Magn. Magn. Mater.* **21**, L198 (1980).

<sup>4</sup>C. F. Majkrzak, J. D. Axe, and P. Böni, *J. Appl. Phys.* **57**, 3657 (1985).

<sup>5</sup>See, for example, *Magnetism of the Zahlenwerte and Funktionen*, in Vol. 9 of *Landolt-Börnstein* edited by K. H. Hellwege and A. M. Hellwege (Springer-Verlag, Berlin, 1962).

<sup>6</sup>M. F. Collins and G. G. Low, *Proc. Phys. Soc. London* **86**, 535 (1965).

<sup>7</sup>J. B. Cowley, T. M. Holden, and G. G. Low, *J. Phys. C* **1**, 458 (1968).

<sup>8</sup>G. Bergmann, *Phys. Rev. Lett.* **41**, 264 (1978).

<sup>9</sup>E. M. Gyorgy, J. F. Dillon, Jr., D. B. McWhan, L. W. Rupp,

Jr., L. R. Testardi, and P. J. Flanders, *Phys. Rev. Lett.* **45**, 57 (1980).

<sup>10</sup>J. Q. Zheng, C. M. Falco, J. B. Ketterson, and I. K. Schuller, *Appl. Phys. Lett.* **38**, 424 (1981).

<sup>11</sup>J. Q. Zhen, J. B. Ketterson, and I. K. Schuller, *J. Appl. Phys.* **53**, 3150 (1982).

<sup>12</sup>A. Arrott and P. E. Noakes, *Phys. Rev. Lett.* **19**, 786 (1967).

<sup>13</sup>W. R. Jones, *J. Appl. Phys.* **53**, 2442 (1982).

<sup>14</sup>D. de Fontaine, in *Local Atomic Arrangements Studied by X-Ray Diffraction*, edited by J. B. Cohen and J. E. Hilliard (Gordon and Breach, New York, 1966).

<sup>15</sup>D. B. McWhan, see Ref. 1.

<sup>16</sup>M. R. Khan, C. S. L. Chun, G. P. Felcher, M. Grimsditch, A. Kueny, C. M. Falco, and I. K. Schuller, *Phys. Rev. B* **27**, 7186 (1983).

<sup>17</sup>As mentioned above, the modulation period can be divided in two parts: the Ni sites that contain a majority of nickel and the Mo sites.